Environmental Pollution 252 (2019) 84–93

Contents lists available at ScienceDirect

Environmental Pollution

journal homepage: www.elsevier.com/locate/envpol

The role of turbulence in internal phosphorus release: Turbulence intensity matters☆

Hong Li [a, *], Guofeng Yang [a], Jianrong Ma [b], Yanyan Wei [c], Li Kang [a], Yixin He [a], Qiang He [a]

[a] Key Laboratory of Eco-Environment of Three Gorges Region, Ministry of Education, Chongqing University, Chongqing, 400044, China
[b] CAS Key Laboratory of Reservoir Environment, Chongqing Institute of Green and Intelligent Technology, Chinese Academy of Sciences, Chongqing, 400714, China
[c] Cultivation Base of Guangxi Key Laboratory for Agro-Environment and Agro-Products Safety, College of Agriculture, Guangxi University, Nanning, 530004, China

ARTICLE INFO

Article history:
Received 10 February 2019
Received in revised form
12 April 2019
Accepted 13 May 2019
Available online 18 May 2019

Keywords:
Sediment-water interface
Phosphorus
Turbulence
Diffusive gradients in thin films (DGT)
Microelectrode

ABSTRACT

Hydrodynamic fluctuations can trigger sediment suspension concomitantly with internal phosphorus release, while the interactive effect of turbulence mixing and sediment suspension on the regulation of phosphorus dynamics is in need of deep understanding. This study addressed the changes in total phosphorus (TP), phosphate (PO_4^{3-}-P) and suspended sediment (SS) in the overlying water, and measured the profile of dissolved oxygen (DO), Fe(II) and soluble reactive phosphorus (SRP) across the sediment-water interface in the simulated environmental turbulence scenario, For a turbulence intensity (ε) of 3.6×10^{-3} m^2/s^3, the SRP flux increased hence PO_4^{3-}-P showed a 36.36% increase relative to its initial level. Although ε of 1.3×10^{-2} m^2/s^3 benefited the delivery of oxygen from the bulk aqueous phase to the upper sediment which can trigger the formation of Fe oxides and hydroxides, the turbulence-induced phosphorus diffusion from the sediment exceeded its inactivation and resulted in a large SRP flux. However, a protion of the released PO_4^{3-}-P can be immobilized through SS adsorption and biotic (likely cyanobacteria) assimilation. Higher turbulence intensities (ε of 3.3×10^{-2} and 7.4×10^{-2} m^2/s^3) led to an approximately 40-fold increase in TP concentration and a significant increase in sediment suspension, which contributed to the immobilization of a majority of the phosphate through adsorption; thus, the PO_4^{3-}-P concentrations in the overlying water displayed 47.75% and 41.67% decline, respectively. This study also confirmed the sequential phosphorus buffer mechanisms associated with increasing turbulence intensities. With an ε of 3.6×10^{-3} m^2/s^3, bounding to Fe ion had a significant impact on phosphorus inactivation but with an ε of 7.4×10^{-2} m^2/s^3, the main immobilization mechanism is switched to phosphorus adsorption from the large quantity of suspended sediment.

1. Introduction

Phosphorus is essential for the support of phytoplankton growth and is a major driving force for water eutrophication (Søndergaard et al., 2013; Conley et al., 2009). Sediment can act as a sources of pollutants in aquatic environments, and the pollutants accumulated in the sediments can be released into the overlying water, contributing a considerable quantity of phosphorus to the water column (Zhang et al., 2018). For most eutrophic waters, the upper 0–10 cm sediment layer typically has much higher phosphorus levels than that is found in the lower sediment layers; and the most heavily contaminated sediment layer is the top 0–5 cm (Tang et al., 2019), where phosphorus is mobile and can be easily released into the overlying water due to changes in the physico-chemical characteristics of the water (Soto-Jimenez et al., 2003; Wu et al., 2001). Thus, even if phosphorus input is effectively reduced, the eutrophication level may remain relatively high, as internal phosphorus loading from sediments may lead to algae blooming and cause a decline in the water quality (Huser and Pilgrim, 2014; Yin et al., 2018; Yin et al., 2016). Therefore, understanding the process of phosphorus release from the sediments is crucial for the management and recovery of eutrophic waters.

The processes underlying the release of internal phosphorus

☆ This paper has been recommended for acceptance by Joerg Rinklebe

* Corresponding author. Chongqing University, 174 Shazheng Street, Shapingba District, Chongqing, 400044, PR China.
E-mail address: hongli@cqu.edu.cn (H. Li).

https://doi.org/10.1016/j.envpol.2019.05.068
0269-7491/

have been extensively explored. Internal phosphorus loading causes an increase in phosphate (PO_4^{3-}-P) levels in water under certain environmental conditions such as pH, redox potential, and hydrodynamic alternations. Iron (Fe) is a redox-sensitive element and its redox cycle plays a primary role in controlling phosphorus mobility in sediments (Ding et al., 2016), which is strongly dependent on the oxygen levels at the sediment-water interface (SWI). The strong adsorption of phosphorus by iron oxyhydroxides in surface sediments can lead to the retention of phosphorus under oxic conditions, whereas the reduction of iron oxyhydroxides under anoxic circumstance can lead to the release of both phosphorus and Fe(II) into the pore water (Petticrew and Arocena, 2001). Oxygen levels across the SWI, which have a significant impact on the forms of Fe, can be regulated a variety of factors. For example, the occurrence of Harmful Algal Blooms causes oxygen depletion at the SWI and triggers the reduction of Fe(III) oxyhydroxides, thereby inducing a release of the Fe-bound phosphorus (Smith et al., 2011).

Turbulence is an intrinsic and ubiquitous characteristic of aquatic environments and can be generated at the surface or can occur by natural processes. Turbulence mixing is a major driver for changes in the physicochemical characteristics of the water column and can, for example, accelerate the oxygen diffuses rate from the atmosphere into the aqueous phase (Chatelain and Guizien, 2010). In addition to facilitating the delivery of oxygen from the water to the surface sediment, turbulence mixing can enhance sediment suspension, which is one of the key processes that influence water turbidity, and indirectly influences eutrophication in shallow lakes (Li et al., 2018). In rives or large shallow lakes, hydrodynamic conditions are often controlled by a combination of wind waves and water flow. These factors enhance the turbulence of the bottom environment, which results in significant sediment resuspension and, potentially, prompt internal phosphorus release (Liu et al., 2019). However, in the Yellow River (China), which has the highest suspended sediment (SS) concentration of any major river in the world, it was found that much of the phosphorus input can be removed by adsorption due to the high SS content (Pan et al., 2013). These studies confirmed that turbulence in aquatic environments can impact the internal phosphorus loading through a variety of processes (e.g., enhanced oxygen delivery and sediment adsorption). Despite these well-documented studies, a coherent theory to explain the impact of turbulence mixing on internal phosphorus loading, particularly the interactive effect of turbulence on oxygen and sediment properties, is still in its infancy.

Here, a 30-day microcosm experiment was conducted in an approximately homogeneous turbulence simulation system (AHTS) to simulate an environmental turbulence scenario. The aim of this study was to: 1) examine the effects of turbulence on phosphorus release from sediment, 2) investigate the potential phosphorus buffer mechanisms under varied turbulence mixing intensities, and 3) identify the dominant processes that influence internal phosphorus release.

2. Material and methods

2.1. Microcosm configuration

The sediment cores and the overlying water used in this study were collected from the estuary of the Yulin River, a tributary of the Yangtze River, China. Due to the interaction between the Yulin River and the main stream of the Yangtze River, the turbulence mixing was strong, as observed in our previous study, which suggested that the turbulent energy dissipation rate (ε, m^2/s^3, describing the turbulence intensity) in the bottom water was in the range of 10^{-3}-10^{-2} m^2/s^3 during the flood season (Kang et al., 2019), which is significantly higher than the wind-induced turbulence intensity in shallow lakes (10^{-8}-10^{-4} m^2/s^3) (Zhu et al., 2018).

Fifteen sediment cores (with sediment heights of approximately 18 cm) were collected using a gravity corer and plexiglass cylinder (with a height of 50 cm and diameter of 11 cm) on 15 May 2018, and water samples were collected simultaneously from the same sites. The primary water physicochemical parameters was the following: DO 6.6–6.8 mg/L, pH 8.26–8.36, turbidity 9.9 NTU, PO_4^{3-}-P 0.05–0.09 mg/L, TP 0.07–0.12 mg/L. Twelve sediment cores were placed in approximately homogeneous turbulence simulation systems (AHTS) to generate the turbulence, with ε of 3.6×10^{-3}, 1.3×10^{-2}, 3.3×10^{-2} and 7.4×10^{-2} m^2/s^3, respectively, with triplicate each. Three additional sediment cores without turbulence mixing were employed as control. The AHTS was constructed from a reactor, a transmission, a motor and a controller (Fig. 1). A grid with square mesh of 0.25 cm^2 was connected to the motor and repeatedly moved vertically, so that the water was pushed back and forth inside the reactor. The jet flow was generated at the edge of the grid and the tail flow was formed above and below the grid, and the interaction between the jet and tail flow generated the approximately isotropic turbulence. The ε value in the AHTS was attained though manipulation of the amplitude and the frequency of the grid, and was estimated following a previous study (Michallet and Mory, 2004):

$$\varepsilon = 0.45\, f^3\, S^2\, (S/M) \quad (1)$$

where f is the grid oscillation frequency, S is the vertical oscillation distance (18.75 cm in this study)and M is the grid mesh size (distance between adjacent bars, 5 mm in this study).

The ZrO-Chelex diffusive gradients in thin films (DGT) devices, which allowed the measurement of parameters at spatial resolutions between submillimeter and millimeter scales, were provided by EasySensor Ltd, Nanjing, China (www.easysensor.net). Prior to deployment in the sediment, the DGT probes were soaked in 0.01M NaCl and deoxygenated using nitrogen for 16 h. Then, the DGT devices were inserted in the sediment cores, with 35 mm exposed

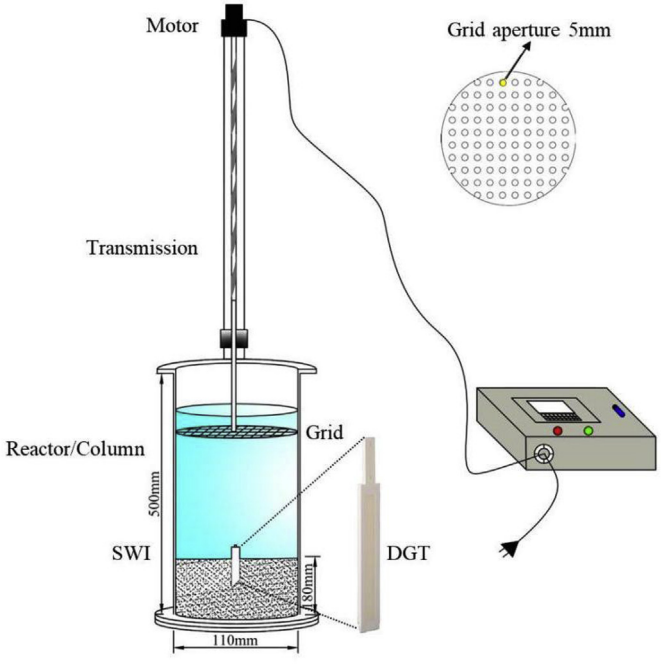

Fig. 1. Illustration of the simulated approximately homogeneous turbulence simulation system (AHTS) in this study.

in the overlying water. After 24 h, the DGT devices were retrieved from the sediments for the subsequent measurements. The DGT devices were used at the beginning and end of each microcosm experiments. After a 30-days incubation and prior to DGT sampling, a needle-type microelectrode system (Unisense, Aarhus, Denmark) with a vertical resolution of 0.05 mm was used to analyze the oxygen distribution across the sediment core.

2.2. Sampling and water analysis

After retrieval, the SWI was marked immediately and the surfaces of the DGT probes were cleaned using deionized water. Then the DGT devices were treated according to the method reported previously (Monbet et al., 2008). Briefly, a slice operation was conducted for the vertical DGT profiles with a vertical resolution of 2 mm. Each gel strip was eluted using 0.25 M H_2SO_4 for phosphorus or 1 M HNO_3 for Fe(II), with a 24 h equilibrium time. The SRP and soluble Fe(II) levels were determined using miniaturized spectrophotometry methods (Epoch Microplate Spectrophotometer, Bio-Tek, Winooski).

During the incubation experiment, 20 ml surface water was collected at 3-day intervals to assess the TP and PO_4^{3-}-P levels. After each sampling, all the studied systems were gently supplied with the original filtered water to compensate for the water losses. The concentrations of TP and PO_4^{3-}-P were measured using the molybdenum blue spectrophotometric method (Han et al., 2015). The pH in the surface water was determined at three-day intervals with a hand-held probe (YSI Professional Plus, USA). Due to sample volume limitations, we measured the water turbidity with a Hach Turbidometer rather than using the total suspended solids (Pearce et al., 2017).

2.3. Sediment analysis

After the 30-day incubation, the surface sediment (0–5 cm) and suspended sediment were separated from the column and stored at −80 °C, and then, with the assistance of Majorbio Bio-Pharm Technology Co. Ltd. (Shanghai, China), high-throughput sequencing analysis was performed to evaluate the response of the microorganism community. The detailed protocols were supplied in Supporting Information (SI). The TP content in the sediment was assessed using the Standards, Measurements and Testing protocol, and the sample was incubated at 720 °C, followed by extraction with 3 M H_2SO_4 (Ruban et al., 2001). Sequential extraction of the phosphorus in frozen dried surface sediment was undertaken to determine the phosphorus species in the surface sediment, as described in the literature (Tang et al., 2018). Briefly, the Occluded phosphorus (O–P), Fe- and Al oxide-bound phosphorus (Fe–P and Al–P, respectively), and calcium-bound phosphorus (Ca–P) were extracted with H_2SO_4: HNO_3:$HClO_4$ (1:2:7), NaOH (1 M) and HCl (1 M), respectively. The Organic phosphorus (Org-P) level was estimated to be the difference between the TP level and the sum of O–P, Fe–P or Al–P, and Ca–P level.

2.4. Data processing

The concentrations of DGT labile SRP and Fe (II) were interpreted as the time-averaged concentration at the device interface (C_{DGT}), as shown by Equation (2).

$$C_{DGT} = \frac{M\Delta g}{DAt} \quad (2)$$

where $\triangle g$ is the thickness of the diffusion layer (cm), D is the analyte diffusion coefficient in the diffusion layer (cm^2/s), t is the deployment time (s), A is the gel exposure area (cm^2), and M is the corresponding accumulated mass over the deployment time (mg).

The net fluxes of the DGT labile SRP and Fe (II) at the SWI are the vectorial sum of the two flux values (Fs and Fw) using Equation (3) (Han et al., 2015)

$$F = Fs + Fw = \left(-\varphi D_s \frac{\vartheta c_s}{\vartheta x_s} \right) + \left(-D_w \frac{\vartheta c_w}{\vartheta x_w} \right) \quad (3)$$

where F is the apparent flux across the SWI ($\mu g/m^2 \bullet d$), Fs and Fw are the fluxes to the sediment and to the overlying water ($\mu g/m^2 \bullet d$), respectively. The bulk sedimentary diffusion coefficients Ds (cm^2/s) were calculated from the molecular diffusion coefficients in water Dw and the porosity (φ). In this study, the Dw = $= 6.32 \times 10^{-6}$ cm^2/s and the Ds = 4.89×10^{-6} cm^2/s for analysis of the SRP flux, and the Dw and Ds are 5.89×10^{-6} and 4.56×10^{-6} cm^2/s for the Fe(II) analysis (Wang et al., 2016; Yu et al., 2017). $\frac{\vartheta c_s}{\vartheta x_s}$ and $\frac{\vartheta c_w}{\vartheta x_w}$ are the concentration gradients in the sediments and overlying water, respectively.

2.5. Statistical analysis

Graphics were obtained using Origin 8.5 software. Significant differences among the treatments were identified through analysis of variance (ANOVA) followed by Tukey's test. The relationships between the DGT labile SRP and Fe (II) were examined through Pearson's correlation method. All statistical analyses were performed in SPSS 19.0, and significance levels were reported at $p < 0.05$ and $p < 0.01$.

3. Results

3.1. Physicochemical properties of overlying waters

In this study, enhanced turbulence intensities induced distinct changes in physicochemical parameters of the overlying waters. In the control and treatment under ε of 3.6×10^{-3} m^2/s^3, the TP concentration (Fig. 2a) and turbidity (Fig. 2c) underwent slight changes. With elevated turbulence intensities, TP concentrations were significantly increased, as the higher turbulence intensities seemed more prone to promote the TP levels. For example, the TP concentrations remained at approximately 0.64 mg/L with ε of 1.3×10^{-2} m^2/s^3 but increased to 4.42 mg/L under ε of 7.4×10^{-2} m^2/s^3 after 30-day incubation. Increases in the PO_4^{3-}-P concentrations were observed in the control and ε of 3.6×10^{-3} m^2/s^3 treatment (displayed 16.32% and 36.36% increases, respectively, during the 30-day study). However, elevated turbulence intensities caused decrease in the PO_4^{3-}-P concentrations, and the reduction rates were 53.19% when the turbulence intensity was 1.3×10^{-2} m^2/s^3 and 47.75% and 41.67% when the turbulence intensities were increased to 3.3×10^{-2} and 7.4×10^{-2} m^2/s^3, respectively (Fig. 2b). The fluctuations of TP concentrations displayed similar patterns in relation to the dynamic of the turbidity (Fig. 2c), and increases of several orders of magnitude in turbidity were recorded in the maximum turbulence intensity groups.

3.2. Microelectrode measurements of oxygen concentration in sediment core

Turbulence led to an apparent change in the oxygen concentration profiles (including DO level and DO penetration depth) in the superficial sediment (Fig. 3). In the studied systems, the DO concentration remained at 202–237 μM in the bulk aqueous phase, and decreased in the diffusive boundary layer above the surface sediment. The DO concentrations at the WI were nearly

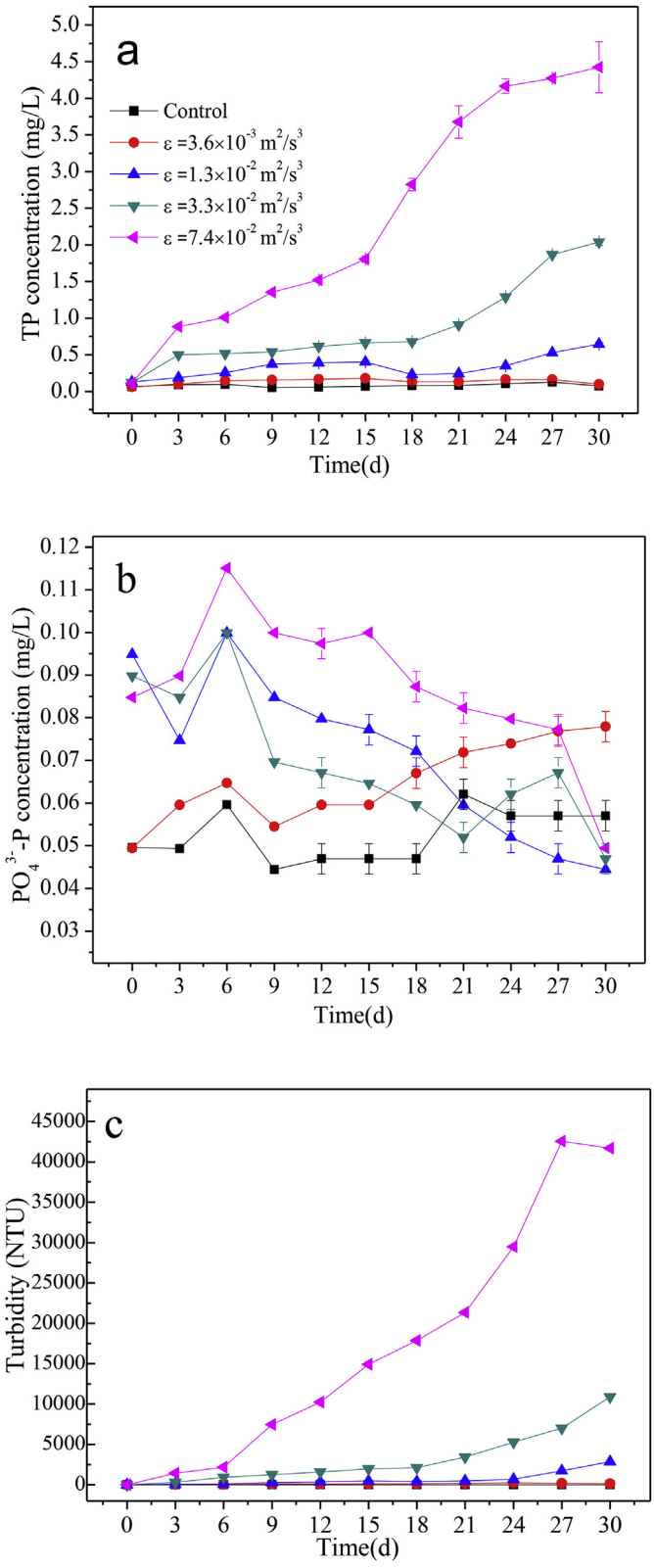

Fig. 2. The dynamics of TP (a), PO_4^{3-}-P (b) and turbidity (c) during the experiment.

identical in the control (Fig. 3) and under a turbulence intensity of 3.6×10^{-3} m^2/s^3, but an increased DO level at the SWI, which maximally reached 237 μM (Fig. 3), was recorded with elevated turbulence intensity. Oxygen penetration was measured up to a

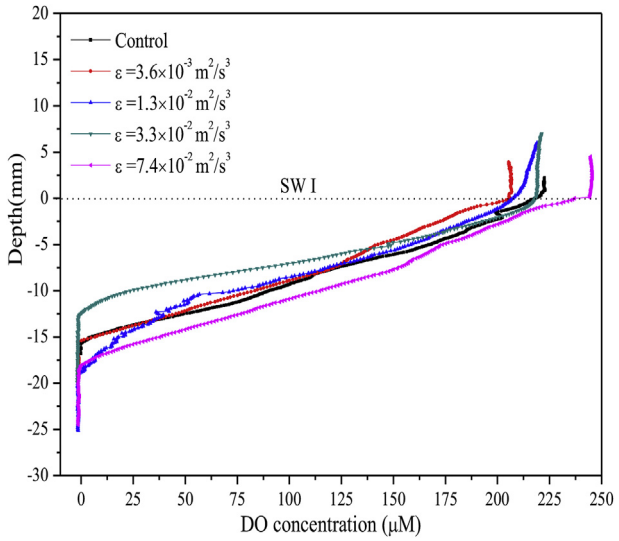

Fig. 3. One-dimensional distribution of DO in the sediment profile after 30 days incubation. All results are expressed as the mean of samples prepared in triplicate at the same depth. a, b, c, d, and e indicate control, turbulence intensity of 3.6×10^{-3}, 1.3×10^{-2}, 3.3×10^{-2} and 7.4×10^{-3} m^2/s^3, respectively. To show the relationship between oxygen concentration and sediment depth more clearly, a depth of 0 on Y-axis was used to represent the sediment-water interface.

depth of ~1.9 mm with an ε of 1.3×10^{-2} m^2/s^3, indicating there was significant oxygen diffusion within the sediment. However, a further increase in the turbulence intensity to 7.4×10^{-3} m^2/s^3 led to a 30.81% decrease in the DO penetration depth (Fig. 3). This may be partly explained by the fact that when the overlying flow is turbulent, the oxygen consumption can be significantly increased as the sediment becomes suspended (Almroth-Rosell et al., 2012).

3.3. Fe (II) and SRP concentration in pore water

The vertical distributions of Fe(II) exhibited similar distribution patterns among the treatments at different water depth, with low concentrations observed in the overlying water and surface sediment, followed by increasing concentrations observed at greater depths. In comparison with its initial concentration, the Fe(II) concentration showed a dramatic increase at a depth of 0–20 mm in the control (from 0.95 mg/L initially to 1.57 mg/L at the end, as shown in Fig. 4a). However, distinct changes in the Fe(II) concentrations under the different turbulence intensities were observed. With a turbulence intensity of 3.6×10^{-3} m^2/s^3, the Fe(II) concentration in the sediment pore water generally reached its maximum at a depth of approximately 10–15 mm (and the Fe(II) concentration was considerably higher than its initial level, indicating there was diffusion of Fe(II) from the deeper sediment to the surface), which then remained stable with increasing sediment depth (Fig. 4b). Although the DO level in the surface sediment in the treatment with a turbulence intensity of 3.6×10^{-3} m^2/s^3 showed slight changes relative to the control, the oxygen penetration depth was increased from 1.38 cm to 1.54 cm (Fig. 3), which favored the production of Fe oxides, and as a result, the Fe(II) concentration below 15 mm were significantly lower than those in the control. Elevation of the turbulence intensity substantially reduced the Fe(II) concentration in the sediment as clearly seen when the turbulence intensity was 1.3×10^{-2} m^2/s^3 (Fig. 4c). Similar trends were also found with ε of 3.3×10^{-2} m^2/s^3 (Fig. 4d). However, further increases in the turbulence intensity had little impact on the Fe(II) concentration (Fig. 4e).

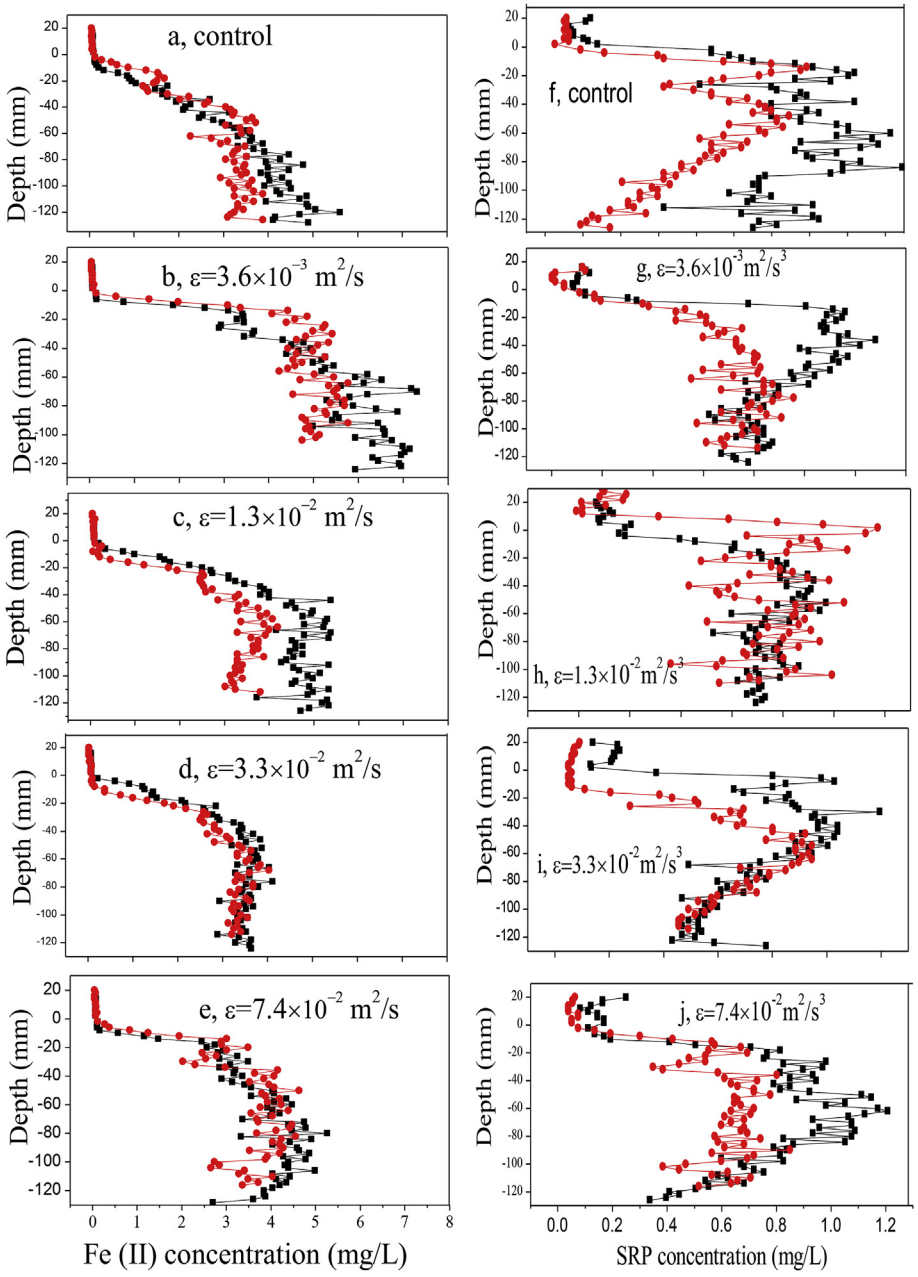

Fig. 4. One-dimensional distribution of Fe (II) (a–e) and DGT labile phosphorus (f–j) in the sediment profile during the incubation. All results are expressed as the mean of triplicate samples from the same depth. The black diamonds indicate the parameters before the experiment and the red correspond to that after 30-days of incubation.

The SRP showed generally low concentrations at depth of 0–20 mm, followed by an increasing trend and then decreasing again with increasing sediment depths. In the control experiments, the depth where increasing concentration was initially observed (D_{ip}) was −4 mm, which did not significantly vary before and after the investigation; further, the depth showing the maximum concentrations (D_{max}) of SRP was −90 mm at the beginning but decreased to −50 mm by the end of the investigation, indicating that phosphorus had been released from the sediment (Fig. 4f). Although D_{ip} did not significantly vary when the turbulence intensity was 3.6×10^{-3} m^2/s^3, the D_{max} increased from −10 mm (initially) to −80 mm (after 30 days), and a linear decrease was exhibited from the SWI to the bottom of the sediment core (Fig. 4g). With ε of 1.3×10^{-2} m^2/s^3, the D_{max} appeared near the SWI after 30 days, in comparison to −40 mm initially, and the SRP concentration in the surface sediment largely exceeded that in the bottom (Fig. 4h), indicating the diffusion of SRP from the sediment. Increasing the turbulence intensity by factors of 2.53 and 5.69 fold resulted in substantial increases in the release of SRP, as indicated by the significantly lower SRP concentration in the pore water after 30 days incubation of incubation compare to its initial level (Fig. 4i and j). Noted that the maximum turbulence intensity in this study (Fig. 4j) diminished the change in the SRP with depth, which indicated there was a drastic SRP releasing or SRP mobilization in the sediment, since D_{max} was seen at a depth of −40 mm and the SRP concentration changed slightly from D_{max} to the bottom. This outcome was distinctly different than the SRP profile under other turbulence intensities.

3.4. SRP and Fe (II) fluxes across SWI

Turbulence can cause a variable release of the SRP from sediment with time (Fig. 5a). Relative to the Fe(II) flux before treatment, turbulence promoted the release of Fe(II), but the releasing rate was depressed with intensified turbulence mixing. During the incubation period, the SRP flux across the SWI increased constantly in both then control and turbulent treatments. The SRP fluxes can be largely enhanced with turbulence intensities from 3.6×10^{-3} and 1.3×10^{-2} m^2/s^3 (for fluxes of 8.98 and 32.94 μg/m^2•d, respectively), but then notably decreased with time with further increase in turbulence intensity (15.31 and 12.63 μg/m^2•d with ε of 3.3×10^{-2} and 7.4×10^{-2} m^2/s^3, respectively). Nevertheless, the SRP fluxes in the turbulent systems uniformly remained positive and were substantially higher than those in the control (6.01 μg/m^2•d, Fig. 5a). Further analysis of the correlation between the SRP and Fe(II) concentrations demonstrated inconsistent patterns under the varied turbulence intensities. Relatively weak turbulence mixing (ε of 3.6×10^{-3} and 1.3×10^{-2} m^2/s^3) induced response of Fe (II) and SRP concentration presented a significant positive correlation (Fig. 5b). In contrast, as the turbulence intensities increase (ε of 3.3×10^{-2} and 7.4×10^{-3} m^2/s^3), the soluble Fe (II) concentrations did not closely correlated with the SRP concentrations (Fig. 5c).

4. Discussion

4.1. Distinct response of aqueous TP and PO_4^{3-}-P dynamics to turbulence mixing

Hydrodynamic alternation often leads to changes in environmental parameters, such as increased sediment resuspension and release of internal nutrients (Kang et al., 2019). A linear increase in TP concentrations with the intensifying turbulence mixing was observed (Fig. 2a). This result agreed well with a previous study which found that relative to the background measurement, the TP concentrations increased by an order of magnitude in the rising flow during a storm event (Chen et al., 2015). However, assessment of the TP concentration does not fully account for the phosphorus release risk associated with its presence in natural waters (Wu et al., 2016) because phosphate is the bioavailable phosphorus fractions. With increases in the turbulence intensity, the release of PO_4^{3-}-P occurred (Fig. 5), while the aqueous PO_4^{3-}-P concentrations exhibited substantial decreases with turbidity intensities of 1.3×10^{-2}, 3.3×10^{-2} and 7.4×10^{-2} m^2/s^3 (Fig. 2b); this clearly demonstrates the distinct response of TP and PO_4^{3-}-P dynamics to turbulence mixing.

The fluctuations in the TP concentrations were closely linked to the turbidity dynamics (Fig. 2c), which was caused from sediment suspension, one of the key processes that indirectly contributes to eutrophication through releasing internal nutrients (Li et al., 2018). Many studies have reported increases in TP following sediment resuspension in lakes but have shown little or no evidence for an increase in SRP (Cyr et al., 2009; You et al., 2007). Although turbulence enhanced SRP release from sediments (Fig. 5a), the phosphate delivered to the waters can be adsorbed by SS particles or be assimilated by the autotrophic and heterotrophic community (Withers and Jarvie, 2008). Despite the significant release of TP under high turbulence intensities (Fig. 2a), there was a reduction in dissolved phosphorus levels in the higher turbulence intensity groups, suggesting the dissolved phosphorus levels can be significantly reduced by a variety of phosphorus buffer mechanisms.

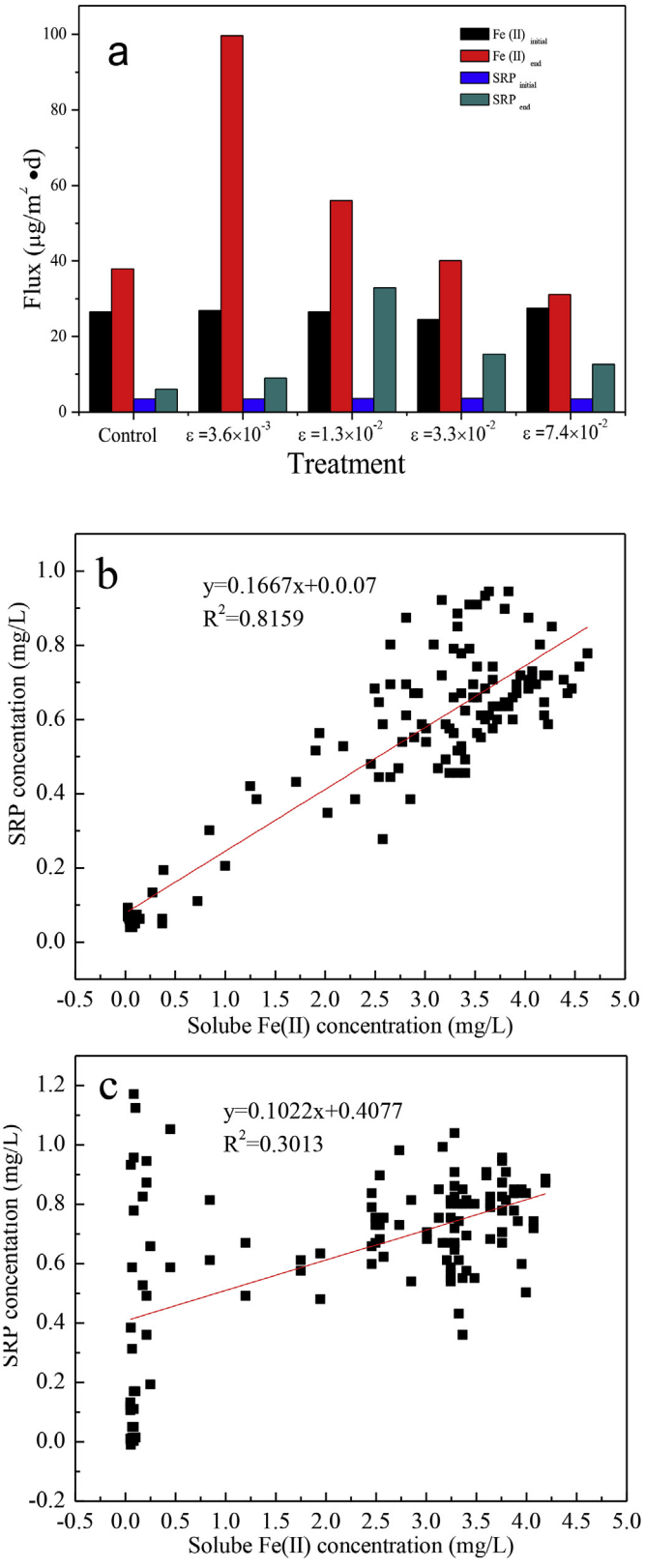

Fig. 5. SRP and Fe(II) diffusion flux across the sediment-water interface at the beginning and end of the study (a) and the correlation between SRP and Fe(II) concentration under varied turbulence intensities. b, the correlation under turbulence intensity of 3.6×10^{-3} and 1.3×10^{-2} m^2/s^3 and c, correlation under turbulence intensity of 3.3×10^{-2} and 7.4×10^{-2} m^2/s^3.

4.2. Multiple approaches for reduction of aqueous PO_4^{3-}-P in turbulent scenario

In natural aquatic systems, there are multiple phosphorus buffer mechanisms that help the aquatic systems regulate the phosphorus concentrations and maintain them at constant levels (Hoffman et al., 2009). Under stable conditions, a balance between the SRP (in the water column) and the loosely bound phosphorus (in the sediments) exists (Lottig and Stanley, 2007), but imbalance would occur if the water experienced hydrodynamic fluctuations. In the current study, turbulence mixing was shown to impact a variety of water parameters, including turbidity (Fig. 2c), DO levels (Fig. 3) and Fe(II) concentrations (Fig. 4a) but there was a less pronounced effect demonstrated by pH (Fig. S1).

Transfer of oxygen across the SWI can regulate biological processes of chemicals in the upper sediment. The oxygen penetration depth, which influences chemical transformations and largely depends on the oxygen consumption in the sediment, increased by 5-fold during turbulent conditions relative to those in static water (Chatelain and Guizien, 2010). The changes in DO levels can trigger multiple biological and physicochemical processes. Many studies support the idea that Fe control phosphorus cycling, with Fe oxides to bound pore water phosphate under aerobic conditions (Herzsprung et al., 2010). In this study, turbulence was found to the penetration of oxygen through the SWI until reaching a depth of several millimeters below the surface layer of sediments (Fig. 3), thus forming a thin oxide layer in which Fe mainly exists in oxidized forms (such as Fe oxides and hydroxides) (Och et al., 2012). This coincided with our observations that the Fe(II) concentrations in the sediment cores showed a linear decrease with increasing turbulence intensity (Fig. 4a–e). In a recent study, it was found that when overlying water was under aerobic conditions, this thin oxide layer on the upper sediments naturally formed an inactivation layer thus hindering the passage of SRP through the SWI and into overlying water (Wang et al., 2019). Hence, the maximum Fe(II) flux caused the minimum release of SRP in the turbulent systems (Fig. 5a). However, the SRP fluxes across the SWI in this study showed that, although elevated turbulence intensities constantly reduced the Fe(II) flux (Fig. 5), the phosphorus release from the sediment was most significant when the turbulence intensity was 1.3×10^{-2} m^2/s^3. Increases or decreases in turbulence intensity can decrease the phosphorus release (Fig. 4f–j and 5a), indicating there are other approaches that impact the phosphorus immobilization in the sediment. This assertion was supported by the correlation analysis between the SRP and Fe(II) concentrations under varied turbulence intensities (Fig. 5b and c), which indicated that relatively weak turbulence mixing caused changes in the Fe (II) and demonstrating that the formation of the Fe–P was the main mechanism for controlling the release of the sediment phosphorus.

In addition to impacting the oxygen diffusion between the bulk solution and the upper sediment, stronger turbulence may cause an increase in the SS concentration (Fig. 2c), which was confirmed by a study evaluating the effects of hydrodynamic disturbances on the resuspension characteristics of sediment (Cheng and Hua, 2016). In the present study, under elevated turbulence intensity, the turbidity showed a constant increase and maximally reached 41700 NTU (Fig. 2c). Previous studies found that sediment resuspension can accelerate the diffusion of pore water nutrients and remobilization of particulate matter, resulting in an increase in particulate and soluble phosphorus in the water column (Wang et al., 2015). However, in our study, although this pattern was found in all of the turbulence intensity gradients studied, the most significant phosphorus release occurred under the turbulence intensity of 1.3×10^{-2} m^2/s^3, further increases in the turbulence intensity appeared to reduce the release of phosphorus, indicating that the turbulence-triggered sediment resuspension may play a vital role. This conclusion was supported by the changes in the TP content of the suspended sediment that were found during the 30-day experiment (Fig. S4) as well as the equilibrium isotherms of the phosphate on the SS (Fig. S2), which indicated that the phosphate was adsorbed onto the SS (Stutter and Lumsdon, 2008). Nevertheless, there was a small release of phosphorus (Fig. 3) with the maximum turbulence intensity in comparison to the control, indicating the release of phosphorus diffusion from the sediment surpasses the Fe oxide inactivation. These findings may be a result of the following: 1) the Fe–P and Org-P phase are considered to be important factors in the buffering of dissolved phosphorus in natural waters (Pan et al., 2013), and in this study, we found the Fe–P accounted for 31.27% of the TP in the control sediment, which can be increased to 34.36–38.69% in the turbulent systems (Fig. S3); this was substantially lower than what was observed in the Nile and Mississippi Rivers (43–46% Fe–P (Pan et al., 2002; Sutula et al., 2004),), and 2) the SS possessed a low adsorption capability toward the phosphorus, as indicated by the theoretical maximum adsorption capacities of PO_4^{3-}-P by the sediment, which was 0.85 mg/g (Fig. S2). The maximum sediment TP content was 0.19 mg/g (Fig. S4), which was nearly 30% of that in Taihu Lake (0.50–0.62 mg/g) (Wu et al., 2019; Zhu et al., 2013). In contrast to the previous assertion that the Fe concentration was the primary factor responsible for the immobilization of phosphorus (Chen et al., 2019), we found that the significantly increased TP concentrations (Fig. 2a) and releasing of SRP from sediment under high turbulence condition (Fig. 5a), accompanied by the substantial increase in SS content (Fig. 2c). This result suggested that the decrease in phosphate levels in the water column was more dependent on the SS content than the phosphorus adsorption capability of the particles, since these particles had very little labile Fe content and showed a low affinity for phosphorus. Therefore, it is likely that the high TP levels in the turbulence treatment were due to the SS absorbed phosphorus; this result is consistent with the previous study, which found that increases in TP were due to the increases in SS (Cyr et al., 2009).

The reduction in PO_4^{3-}-P was generally attributed to rapid phosphorus adsorption by the SS, and uptake by bacteria and algae may contribute to the reduction as well (Cyr et al., 2009). After the 30-day incubation, the content of mobile-P (the sum of Fe–P and Org-P, which contributed a lot to the sediment internal phosphorus loading in eutrophic lakes) accounted for 52–57% of the TP in the turbulence systems and 48.45% of the TP in the control treatment (Fig. S3), indicting the released mobile-P may facilitate phytoplankton assimilation. Consequently, the relative abundances of *cyanobacteria* were increased by 9.57% with a turbulence intensity of 1.3×10^{-2} m^2/s^3 relative to that in control, indicating the turbulence may facilitate the release of internal nutrients release and consequently benefit phytoplankton growth; this may in turn contribute to the biotic assimilation of PO_4^{3-}-P. When the turbulence intensity further reached 7.4×10^{-2} m^2/s^3, the relative abundances of *cyanobacteria* decreased to 4.43%, presumably due to the light attenuation, as extremely high turbidity deteriorated phytoplankton growth (Fig. S5).

4.3. Switching of phosphorus buffer mechanism under varied turbulence intensities

Under the studied turbulence intensity levels (3.6×10^{-3} - 7.4×10^{-2} m^2/s^3), the DO concentrations at the SWI, the oxygen penetration depth, the sediment suspension and Fe(II) concentrations showed dramatic responses, which were the potential buffer mechanisms of phosphorus immobilization in the turbulent water. However, the responses of the parameters that closely associated

with phosphorus dynamics showed distinct differences with the increases in turbulence intensities. For example, the increase in turbidity, which is essential for phosphorus adsorption, is most obvious with a turbulence intensity of 7.4×10^{-2} m^2/s^3 (Fig. 2c); however, the maximum DO penetration depth, which implying the improvement in DO diffusion from aqueous phase to surface sediment, occurs with a turbulence intensity of 1.3×10^{-2} m^2/s^3 (Fig. 3). The observed changes in the parameters indicated that the phosphorus buffer mechanism varied with changes in the turbulence intensity. A turbulence intensity of 3.6×10^{-3} m^2/s^3 caused a 36.36% increase in PO_4^{3-}-P in the water phase compared to its initial level, suggesting that the phosphorus inactivation may be much less consequential than the phosphorus diffusion from the sediment. Increasing the turbulence intensity by 3.6-fold favored the diffusion of oxygen from the bulk aqueous phase to sediment and triggered the formation of Fe oxides and hydroxides, but the inactivation of phosphorus to Fe oxides seemed a litter weak than phosphorus diffusion from the sediment; however, phytoplankton growth may consume the phosphate. In contrast to the previous study, which generally reported phosphorus release under hydrodynamic shift conditions, we found that, although further increasing the turbulence intensity to 3.3×10^{-2} and 7.4×10^{-2} m^2/s^3 resulted in the phosphorus diffusion outcompeting phosphorus inactivation (as indicated by the positive SRP flux across the sediment-water interface), the released phosphorus was mostly adsorbed by the suspended sediment, and a large decrease in the PO_4^{3-}-P levels was recorded (a nearly 50% reduction). Due to the combination of these effects, the aqueous PO_4^{3-}-P concentration was decreased with the turbulence intensity of 1.3×10^{-2} – 7.4×10^{-2} m^2/s^3, despite the positive SRP flux. The potential process underlying the differing phosphorus immobilization processes under varied turbulence mixing levels is described in Fig. 6.

4.4. Environmental implications

Various factors can influence the release of internal phosphorus across the SWI, such as DO saturation, pH, Fe(III)/P, and resuspension (Huang et al., 2016; Liu et al., 2016). It had been found that phosphorus can be released into the overlying water in both the dissolved and particulate phases, and the release rate is directly related to the intensity of the sediment disturbance (Wang et al., 2009). In this study, we confirmed that turbulence mixing induced the release of SRP and reduced the PO_4^{3-}-P levels primarily through SS adsorption. Accordingly, the suspended sediment acted as a sink for additional phosphate, and this effect was due to the high SS content in turbulent water rather than the surface activity of the particles. But it should be note that the TGR has experienced significant reduction in sediment discharge since its completion (He et al., 2018), and the SS content showed further reduction due to anthropogenic activities; this indicates that the phosphate will likely be increased and there may be irreversible water quality problems (e.g., eutrophication) in this large ecological system. The result of this study also contributes to a better understanding of the role that suspended sediment content plays in the improvement of water quality and the control of phytoplankton blooms. Through the implementation of a hydrodynamic approach in river, e.g., appropriate control of river discharge, or manipulating the waves in lakes, which could regulate the SS content, the bioavailable phosphorus could potentially be controlled.

5. Conclusions

This study investigated phosphorus immobilization in the bulk aqueous phase and sediment core in response to turbulence mixing. A turbulence intensity of 3.6×10^{-3} m^2/s^3 caused a slight variation in the TP concentration but caused a 36.36% increase of PO_4^{3-}-P in the water phase. Increasing the turbulence intensity by 3.6-fold favored the diffusion of oxygen from the bulk aqueous phase to the sediment and triggered the formation of Fe oxides and hydroxides; however, the inactivation of phosphorus toward Fe was less consequential than phosphorus diffusion from the sediment, resulting in a significant release of phosphorus into the overlying water. In contrast with the previous study, which generally reported phosphorus release in hydrodynamic shift conditions, we found that further increasing the turbulence intensity caused a substantial suspension of the sediment. As a result, the main process for phosphorus immobilization became phosphorus adsorption, during which the low labile Fe content and low affinity for phosphorus indicated a large quantity of suspended sediment was imperative for PO_4^{3-}-P reduction. To our knowledge, this is the first study to confirm that the main phosphorus buffer mechanism changed from Fe oxide binding to suspended sediment adsorption under elevated turbulence intensities, which eventually causes a decrease rather than an increase in the phosphate; thus, this work has potential to contribute new knowledge to the current understanding of phosphorus immobilization in turbulent waters.

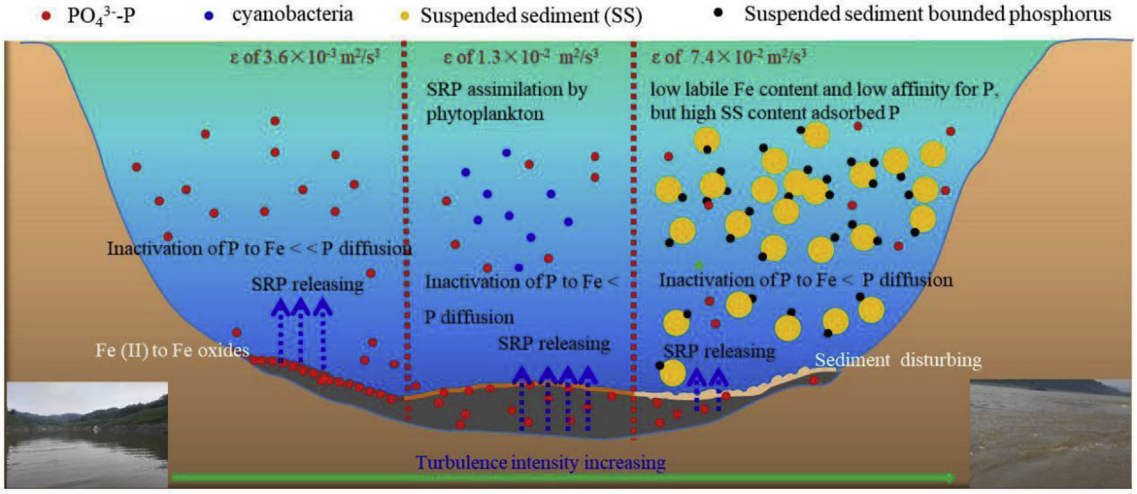

Fig. 6. Conceptual schematic of the synergistic effects of turbulence on phosphorus dynamic.

Acknowledgments

This work was jointly supported by the Natural Science Foundation of China (NSFC 51609024, 41877472, 41401574 and 41601537), and Chongqing Research Program of Basic Research and Frontier Technology (cstc2016jcyjA0498 and cstc2018jcyjAX0601), and Fundamental Research Funds for the Central Universities (2019CDQYCH013and 2018CDXYCH0014).

Appendix A. Supplementary data

Supplementary data to this article can be found online at https://doi.org/10.1016/j.envpol.2019.05.068.

Conflicts of interest

The authors declare no competing financial interest.

References

Almroth-Rosell, E., Tengberg, A., Andersson, S., Apler, A., Hall, P.O.J., 2012. Effects of simulated natural and massive resuspension on benthic oxygen, nutrient and dissolved inorganic carbon fluxes in Loch Creran. Scotland. J. Sea Res. 72, 38–48. https://doi.org/10.1016/j.seares.2012.04.012.

Chatelain, M., Guizien, K., 2010. Modelling coupled turbulence-Dissolved oxygen dynamics near the sediment–water interface under wind waves and sea swell. Water Res. 44, 1361–1372. https://doi.org/10.1016/j.watres.2009.11.010.

Chen, M., Ding, S., Wu, Y., Fan, X., Jin, Z., Tsang, D.C.W., Wang, Y., Zhang, C., 2019. Phosphorus mobilization in lake sediments: experimental evidence of strong control by iron and negligible influences of manganese redox reactions. Environ. Pollut. 246, 472–481. https://doi.org/10.1016/j.envpol.2018.12.031.

Chen, N., Wu, Y., Chen, Z., Hong, H., 2015. Phosphorus export during storm events from a human perturbed watershed, southeast China: implications for coastal ecology. Estuar. Coast Shelf Sci. 166, 178–188. https://doi.org/10.1016/j.ecss.2015.03.023.

Cheng, H., Hua, Z., 2016. Effects of hydrodynamic disturbances and resuspension characteristics on the release of tetrabromobisphenol A from sediment. Environ. Pollut. 219, 785–793. https://doi.org/10.1016/j.envpol.2016.07.055.

Conley, D.J., Paerl, H.W., Howarth, R.W., Boesch, D.F., Seitzinger, S.P., Havens, K.E., Lancelot, C., Likens, G.E., 2009. Controlling eutrophication: nitrogen and phosphorus. Science 323, 1014. https://doi.10.1126/science.1167755.

Cyr, H., McCabe, S.K., Nürnberg, G.K., 2009. Phosphorus sorption experiments and the potential for internal phosphorus loading in littoral areas of a stratified lake. Water Res. 43, 1654–1666. https://doi.org/10.1016/j.watres.2008.12.050.

Ding, S., Wang, Y., Wang, D., Li, Y.Y., Gong, M., Zhang, C., 2016. In situ, high-resolution evidence for iron-coupled mobilization of phosphorus in sediments. Sci. Rep. 6, 24341. https://www.nature.com/articles/srep24341.

Han, C., Ding, S., Yao, L., Shen, Q., Zhu, C., Wang, Y., Xu, D., 2015. Dynamics of phosphorus–iron–sulfur at the sediment–water interface influenced by algae blooms decomposition. J. Hazard Mater. 300, 329–337.

He, Q., Kang, L., Sun, X., Jia, R., Zhang, Y., Ma, J., Li, H., Ai, H., 2018. Spatiotemporal distribution and potential risk assessment of microcystins in the Yulin River, a tributary of the Three Gorges Reservoir, China. J. Hazard Mater. 347, 184–195. https://doi.org/10.1016/j.jhazmat.2015.07.009.

Herzsprung, P., Schultze, M., Hupfer, M., Boehrer, B., Tümpling, W.V., Duffek, A., Van der Veen, A., Friese, K., 2010. Flood effects on phosphorus immobilisation in a river water filled pit lake—case study Lake Goitsche (Germany). Limnologica 40, 182–190. https://doi.org/10.1016/j.limno.2009.11.007.

Hoffman, A.R., Armstrong, D.E., Lathrop, R.C., Penn, M.R., 2009. Characteristics and influence of phosphorus accumulated in the bed sediments of a stream located in an agricultural watershed. Aquat. Geochem. 15, 371–389. https://link.springer.com/article/10.1007/s10498-008-9043-2.

Huang, L., Fang, H., He, G., Jiang, H., Wang, C., 2016. Effects of internal loading on phosphorus distribution in the Taihu Lake driven by wind waves and lake currents. Environ. Pollut. 219, 760–773. https://doi.org/10.1016/j.envpol.2016.07.049.

Huser, B.J., Pilgrim, K.M., 2014. A simple model for predicting aluminum bound phosphorus formation and internal loading reduction in lakes after aluminum addition to lake sediment. Water Res. 53, 378–385. https://doi.org/10.1016/j.watres.2014.01.062.

Kang, L., He, Y., Dai, L., He, Q., Ai, H., Yang, G., Liu, M., Jiang, W., Li, H., 2019. Interactions between suspended particulate matter and algal cells contributed to the reconstruction of phytoplankton communities in turbulent waters. Water Res. 149, 251–262. https://doi.org/10.1016/j.watres.2018.11.003.

Li, Y., Wei, J., Gao, X., Chen, D., Weng, S., Du, W., Wang, W., Wang, J., Tang, C., Zhang, S., 2018. Turbulent bursting and sediment resuspension in hyper-eutrophic Lake Taihu, China. J. Hydrol 565, 581–588. https://doi.org/10.1016/j.jhydrol.2018.08.067.

Liu, C., Du, Y., Yin, H., Fan, C., Chen, K., Zhong, J., Gu, X., 2019. Exchanges of nitrogen and phosphorus across the sediment-water interface influenced by the external suspended particulate matter and the residual matter after dredging. Environ. Pollut. 246, 207–216. https://doi.org/10.1016/j.envpol.2018.11.092.

Liu, C., Shao, S., Shen, Q., Fan, C., Zhang, L., Zhou, Q., 2016. Effects of riverine suspended particulate matter on the post-dredging increase in internal phosphorus loading across the sediment-water interface. Environ. Pollut. 211, 165–172. https://doi.org/10.1016/j.envpol.2015.12.045.

Lottig, N.R., Stanley, E.H., 2007. Benthic sediment influence on dissolved phosphorus concentrations in a headwater stream. Biogeochemistry 84, 297–309. https://link.springer.com/article/10.1007/s10533-007-9116-0.

Michallet, H., Mory, M., 2004. Modelling of sediment suspensions in oscillating grid turbulence. Fluid Dyn. Res. 35, 87–106. https://iopscience.iop.org/article/10.1016/j.fluiddyn.2004.04.004/meta.

Monbet, P., McKelvie, I.D., Worsfold, P.J., 2008. Combined gel probes for the in situ determination of dissolved reactive phosphorus in porewaters and characterization of sediment reactivity. Environ. Sci. Technol. 42, 5112–5117. https://pubs.acs.org.ccindex.cn/doi/abs/10.1021/es8001663.

Och, L.M., Müller, B., Voegelin, A., Ulrich, A., Göttlicher, J., Steiniger, R., Mangold, S., Vologina, E.G., Sturm, M., 2012. New insights into the formation and burial of Fe/Mn accumulations in Lake Baikal sediments. Chem. Geol. 330–331, 244–259. https://doi.org/10.1016/j.chemgeo.2012.09.011.

Pan, G., Krom, M.D., Herut, B., 2002. Adsorption– desorption of phosphate on airborne dust and riverborne particulates in East Mediterranean seawater. Environ. Sci. Technol. 36, 3519–3524. https://pubs.acs.org.ccindex.cn/doi/abs/10.1021/es020516d.

Pan, G., Krom, M.D., Zhang, M., Zhang, X., Wang, L., Dai, L., Sheng, Y., Mortimer, R.J.G., 2013. Impact of suspended inorganic particles on phosphorus cycling in the Yellow River (China). Environ. Sci. Technol. 47, 9685–9692. https://pubs.acs.org.ccindex.cn/doi/pdf/10.1021/es4005619.

Pearce, A.R., Chambers, L.G., Hasenmueller, E.A., 2017. Characterizing nutrient distributions and fluxes in a eutrophic reservoir, Midwestern United States. Sci. Total Environ. 581–582, 589–600. https://doi.org/10.1016/j.scitotenv.2016.12.168.

Petticrew, E.L., Arocena, J.M., 2001. Evaluation of iron-phosphate as a source of internal lake phosphorus loadings. Sci. Total Environ. 266, 87–93. https://doi.org/10.1016/S0048-9697(00)00756-7.

Ruban, V., Lopez-Sanchez, J.F., Pardo, P., Rauret, G., Muntau, H., Quevauviller, P., 2001. Development of a harmonised phosphorus extraction procedure and certification of a sediment reference material. J. Environ. Monit. 3, 121–125. https://pubs.rsc.org/en/content/articlehtml/2001/em/b005672n.

Smith, L., Watzin, M.C., Druschel, G., 2011. Relating sediment phosphorus mobility to seasonal and diel redox fluctuations at the sediment–water interface in a eutrophic freshwater lake. Limnol. Oceanogr. 56, 2251–2264. https://doi.org/10.4319/lo.2011.56.6.2251.

Søndergaard, M., Bjerring, R., Jeppesen, E., 2013. Persistent internal phosphorus loading during summer in shallow eutrophic lakes. Hydrobiologia 710, 95–107. https://link.springer.com/article/10.1007/s10750-012-1091-3.

Soto-Jimenez, M.F., Paez-Osuna, F., Bojorquez-Leyva, H., 2003. Nutrient cycling at the sediment–water interface and in sediments at Chiricahueto marsh: a subtropical ecosystem associated with agricultural land uses. Water Res. 37, 719–728. https://doi.org/10.1016/S0043-1354(02)00380-9.

Stutter, M.I., Lumsdon, D.G., 2008. Interactions of land use and dynamic river conditions on sorption equilibria between benthic sediments and river soluble reactive phosphorus concentrations. Water Res. 42, 4249–4260. https://doi.org/10.1016/j.watres.2008.06.017.

Sutula, M., Bianchi, T.S., McKee, B.A., 2004. Effect of seasonal sediment storage in the lower Mississippi River on the flux of reactive particulate phosphorus to the Gulf of Mexico. Limnol. Oceanogr. 49, 2223–2235. https://doi.org/10.4319/lo.2004.49.6.2223.

Tang, X., Li, R., Wu, M., Zhao, W., Zhao, L., Zhou, Y., Bowes, M.J., 2019. Influence of turbid flood water release on sediment deposition and phosphorus distribution in the bed sediment of the Three Gorges Reservoir, China. Sci. Total Environ. 657, 36–45. https://doi.org/10.1016/j.scitotenv.2018.12.011.

Tang, X., Wu, M., Li, R., 2018. Phosphorus distribution and bioavailability dynamics in the mainstream water and surface sediment of the Three Gorges Reservoir between 2003 and 2010. Water Res. 145, 321–331. https://doi.org/10.1016/j.watres.2018.08.041.

Wang, J., Chen, J., Chen, Q., Yang, H., Zeng, Y., Yu, P., Jin, Z., 2019. Assessment on the effects of aluminum-modified clay in inactivating internal phosphorus in deep eutrophic reservoirs. Chemosphere 215, 657–667. https://doi.org/10.1016/j.chemosphere.2018.10.095.

Wang, P., Hu, B., Wang, C., Lei, Y., 2015. Phosphorus adsorption and sedimentation by suspended sediments from zhushan bay, Taihu Lake. Environ. Sci. Pollut. Res. 22, 6559–6569. https://link.springer.com/article/10.1007/s11356-015-4114-6.

Wang, S., Jin, X., Zhao, H., Wu, F., 2009. Phosphorus release characteristics of different trophic lake sediments under simulative disturbing conditions. J. Hazard Mater. 161, 1551–1559. https://doi.org/10.1016/j.jhazmat.2008.05.004.

Wang, Y., Ding, S., Gong, M., Xu, S., Xu, W., Zhang, C., 2016. Diffusion characteristics of agarose hydrogel used in diffusive gradients in thin films for measurements of cations and anions. Anal. Chim. Acta 945, 47–56. https://doi.org/10.1016/j.aca.2016.10.003.

Withers, P.J.A., Jarvie, H.P., 2008. Delivery and cycling of phosphorus in rivers: a review. Sci. Total Environ. 400, 379–395. https://doi.org/10.1016/j.scitotenv.2008.08.002.

Wu, F., Qing, H., Wan, G., 2001. Regeneration of N, P and Si near the sediment/water

interface of lakes from Southwestern China Plateau. Water Res. 35, 1334–1337. https://doi.org/10.1016/S0043-1354(00)00380-8.

Wu, T., Qin, B., Brookes, J.D., Yan, W., Ji, X., Feng, J., 2019. Spatial distribution of sediment nitrogen and phosphorus in Lake Taihu from a hydrodynamics-induced transport perspective. Sci. Total Environ. 650, 1554–1565. https://doi.org/10.1016/j.scitotenv.2018.09.145.

Wu, Y., Wang, X., Zhou, J., Bing, H., Sun, H., Wang, J., 2016. The fate of phosphorus in sediments after the full operation of the Three Gorges Reservoir, China. Environ. Pollut. 214, 282–289. https://doi.org/10.1016/j.envpol.2016.04.029.

Yin, H., Douglas, G.B., Cai, Y., Liu, C., Copetti, D., 2018. Remediation of internal phosphorus loads with modified clays, influence of fluvial suspended particulate matter and response of the benthic macroinvertebrate community. Sci. Total Environ. 610–611, 101–110. https://doi.org/10.1016/j.scitotenv.2017.07.243.

Yin, H., Han, M., Tang, W., 2016. Phosphorus sorption and supply from eutrophic lake sediment amended with thermally-treated calcium-rich attapulgite and a safety evaluation. Chem. Eng. J. 285, 671–678. https://doi.org/10.1016/j.cej.2015.10.038.

You, B.S., Zhong, J.C., Fan, C.X., Wang, T.X., Zhang, L., Ding, S.M., 2007. Effects of hydrodynamics processes on phosphorus fluxes from sediment in large, shallow Taihu Lake. J. Environ. Sci. 19, 1055–1060. https://doi.org/10.1016/S1001-0742(07)60172-7.

Yu, J., Ding, S., Zhong, J., Fan, C., Chen, Q., Yin, H., Zhang, L., Zhang, Y., 2017. Evaluation of simulated dredging to control internal phosphorus release from sediments: focused on phosphorus transfer and resupply across the sediment-water interface. Sci. Total Environ. 592, 662–673. https://doi.org/10.1016/j.scitotenv.2017.02.219.

Zhang, W., Jin, X., Meng, X., Tang, W., Shan, B., 2018. Phosphorus transformations at the sediment–water interface in shallow freshwater ecosystems caused by decomposition of plant debris. Chemosphere 201, 328–334. https://doi.org/10.1016/j.chemosphere.2018.03.006.

Zhu, L., Qin, B., Zhou, J., Van Dam, B., Shi, W., 2018. Effects of turbulence on carbon emission in shallow lakes. J. Environ. Sci. 69, 166–172. https://doi.org/10.1016/j.jes.2017.10.005.

Zhu, M., Zhu, G., Li, W., Zhang, Y., Zhao, L., Gu, Z., 2013. Estimation of the algal-available phosphorus pool in sediments of a large, shallow eutrophic lake (Taihu, China) using profiled SMT fractional analysis. Environ. Pollut. 173, 216–223. https://doi.org/10.1016/j.envpol.2012.10.016.